

Dalton Transactions

Accepted Manuscript



This is an *Accepted Manuscript*, which has been through the Royal Society of Chemistry peer review process and has been accepted for publication.

Accepted Manuscripts are published online shortly after acceptance, before technical editing, formatting and proof reading. Using this free service, authors can make their results available to the community, in citable form, before we publish the edited article. We will replace this *Accepted Manuscript* with the edited and formatted *Advance Article* as soon as it is available.

You can find more information about *Accepted Manuscripts* in the [Information for Authors](#).

Please note that technical editing may introduce minor changes to the text and/or graphics, which may alter content. The journal's standard [Terms & Conditions](#) and the [Ethical guidelines](#) still apply. In no event shall the Royal Society of Chemistry be held responsible for any errors or omissions in this *Accepted Manuscript* or any consequences arising from the use of any information it contains.

Synthesis, structure, spectral and electrochemical properties of chromium(III) *tris*-(8-hydroxyquinolate)[†]

Ana R. Freitas,^a Mónica Silva,^a M. Luísa Ramos,^a Licínia L. G. Justino,^a Sofia M. Fonseca,^a Madalina M. Barsan,^b Christopher M. A. Brett,^b M. Ramos Silva,^c Hugh D. Burrows*^a

^a*Centro de Química and Department of Chemistry, University of Coimbra, 3004-535 Coimbra, Portugal. Email: burrows@ci.uc.pt; Fax: +351+239827703; Tel. +351+239854482*

^b*Department of Chemistry, University of Coimbra, 3004-535 Coimbra, Portugal*

^c*CEMDRX, Department of Physics, University of Coimbra, 3004-516 Coimbra, Portugal*

[†] Electronic supplementary information (ESI) available

ABSTRACT

The kinetically inert chromium(III) *tris*-(8-hydroxyquinolate), Crq₃, has been synthesized, crystallized from 90% methanol-water, and characterized by MALDI-TOF mass spectrometry, thermogravimetry, FTIR, NMR spectroscopy, and X-ray powder diffraction. It is formed as a methanol solvate, but solvent can be removed by heating. Large paramagnetic shifts and spectral broadening in ¹H NMR spectra indicate electron delocalization between metal and ligand. DFT calculations show it is present as the *meridional* isomer, with the HOMO largely based on one of the metal 3d orbitals and the LUMO essentially localized on the ligands. Cyclic voltammetry (CV) in acetonitrile solutions shows four oxidation peaks and two, less intense reduction waves on first scan. The HOMO energy determined from the first oxidation peak is fairly close to that obtained by DFT, in agreement with this being mainly metal based. Although the number of peaks decreases on subsequent CV scans, the complex shows markedly enhanced electrochemical stability compared with aluminium(III) *tris*-(8-hydroxyquinolate). Solution UV/visible absorption and solid diffuse reflectance spectra have a weak, long wavelength band, assigned to the metal based d-d transition, in addition to the normal, ligand based, bands seen in metal quinolates. The energy of the lowest energy band is identical to the HOMO-LUMO separation obtained by cyclic voltammetry, in agreement with the above description. The compound is only weakly luminescent, in contrast to many other metal quinolates, due to the lowest energy transition being metal rather than ligand based. The potential of this compound as an electron transporting/hole blocking layer in optoelectronic devices is indicated.

1. Introduction

Metal complexes of 8-hydroxyquinoline (sometimes termed oxinates) have been known for over a century.¹ Complexes of 8-hydroxyquinoline and its derivatives with metal ions have found extensive use in analytical chemistry in areas such as optical (particularly fluorescence) sensing,²⁻⁵ and were, formerly, extensively used in gravimetric analysis of metals.^{6,7} The 8-hydroxyquinolate (8-Hq) ligand is a selective sorbent of toxic metals.⁸ Metal complexes of 8-Hq have also found biomedical applications, including tumour growth inhibitors in cancer treatment,^{9,10} and imaging agents in positron emission tomography (PET).¹¹ Supramolecular coordination compounds of 8-Hq and its derivatives are particularly promising for some of these applications.¹² However, probably the major use of metal quinolates at present is as light emitting and/or electron-transport layers in organic light emitting devices (OLEDs). This stems from the original observation of efficient electroluminescence from aluminium(III) quinolate (Alq₃) by Tang and van Slyke in 1987,¹³ and forms the basis of a multibillion Euro industry in displays for laptops, tablets and televisions. In addition to these applications, OLEDs are likely to be major candidates for the next generation of solid-state white lighting.¹⁴ Electron transporting properties of aluminium quinolates also find applications in photovoltaic devices.¹⁵

Device efficiency of a molecule in these organic electronic systems depends on its highest occupied (HOMO) and lowest unoccupied molecular orbital (LUMO) energy levels. The development of Alq₃ as one of the most studied metal chelate for application in OLEDs stems from its high electron affinity (E_A) and ionization potential (I_P) values.¹⁶ Cyclic voltammetry (CV) provides a convenient method to determine the oxidation and reduction potentials and, hence, the HOMO and LUMO levels in condensed phases. The oxidation process corresponds to the removal of one electron from the HOMO molecular orbital, so that the potential E_{ox} at which oxidation reaction occur in CV is directly correlated with the energy required to extract the electron from the molecule. In a similar way, reduction peak potentials are used to determine the energy level of LUMO, which is the energy necessary to inject an electron into a molecule. The determination of HOMO and LUMO energies from CV data is obtained using the correlations discussed by Bredas *et al.*,¹⁷ and expressed as:

$$E_{HOMO} = -e [E_{ox} + 4.4], (1)$$

$$E_{\text{LUMO}} = -e [E_{\text{red}} + 4.4] \quad (2)$$

It is known that in an OLED, or other optoelectronic system, the electron affinity (E_{A}) or E_{LUMO} level and the ionization potential (I_{P}) or E_{HOMO} level, relative to the cathode work function and the anode work function, respectively, determine the charge injection into the diode. Large energy barriers between HOMO and LUMO lead to poor OLED performance.¹⁸ In addition, it has been demonstrated that the molecular orbitals localized on hydroxyquinolate ligand are those that dictate the electroluminescence of Alq₃.¹⁹

However, these excellent electronic characteristics are tempered by the fact that Alq₃ degrades upon one-electron oxidation, which limits long term stability of its optoelectronic devices.^{20,21} Matrix assisted laser desorption/ionization time-of-flight mass spectrometry studies on Alq₃, show that ionization (i.e. one electron oxidation or hole formation) results in ligand loss to form the Alq₂⁺ species, which may undergo dimerization or other processes.²² Although in the thin layers involved in solid state devices, the ligand cannot readily diffuse through the film layers, allowing the possibility of its recombination with the Al(III) centre, in the long term, the instability of the radical cation will lead to degradation and a decrease in the device lifetime. There is, thus, a strong incentive for developing alternative materials.

Chromium(III) and aluminium(III) have very similar ionic radii, coordination numbers (typically six), and their complexes have comparable thermodynamic stabilities.²³ There are, however, two important differences. Firstly, while aluminium only shows a single stable trivalent oxidation state (Al(III)), the chromium metal ion can exist in a wide variety of oxidation states, with the one electron oxidized (Cr(IV)) and reduced (Cr(II)) states obtained from chromium(III) being stable and readily accessible, in energetic terms.²⁴ In addition, while Al(III) complexes fairly rapidly undergo ligand exchange, the 3d³ electronic configuration of chromium(III) makes its complexes kinetically inert to substitution, with rates at least a million times slower than those of the corresponding aluminium(III) complexes.^{23,25,26}

Chromium(III) complexes also show interesting electronic spectral properties, involving metal based quartet and doublet states, together with ligand based π, π^* states, and, possibly, charge transfer states, as demonstrated by detailed UV/visible absorption,²⁷ luminescence spectral,^{28,29} and photophysical studies.^{30,31} In one case, electrogenerated

chemiluminescence has been observed with a chromium(III) complex.³² The above characteristics make chromium(III) quinolates good candidates for further study for optoelectronic applications.

Further interest in stable chromium(III) complexes stems from their paramagnetic character. The development of nuclear magnetic resonance image techniques as a clinical diagnostic modality has prompted the need for a new class of pharmaceuticals to enhance the image contrast between normal and diseased tissue or indicate the status of organ function or blood flow. The image intensity in ¹H NMR imaging, largely composed of the NMR signal of water protons, is dependent on nuclear relaxation times. Complexes of lanthanide ions, e.g. Gd(III), which can decrease the relaxation times of nearby nuclei via dipolar interactions, have received the most attention as contrast agents.^{33,34} The important properties related with the ¹H fast relaxation of nearby nuclei of the Cr(III) complexes and their spherical symmetry may also make them good potential candidates for use as relaxation agents having potential application in magnetic resonance imaging (MRI).

For the above reasons, we have carried out a detailed structural, spectral and electrochemical study on chromium(III) 8-hydroxyquinolate (Crq₃). Although chromium(III) 8-hydroxyquinolate was first reported in 1938,³⁵ reliable results on its synthesis and characterization have been fairly sporadic,^{6,36-44} and it is only recently that relatively detailed structural data on this compound has been reported.⁴⁵ In part, this stems from the same kinetic inertness that makes this material interesting for device applications. In addition, Crq₃ tends to crystallize as a solvate.^{36,46} Following from our earlier studies on the water soluble derivative 8-hydroxyquinoline-5-sulfonate (8-HqS) with the trivalent cations Al(III),^{47,48} we initially studied standard routes to Crq₃ synthesis by looking at the reaction of the water soluble 8-HqS with chromium(III) in aqueous solutions. However, no significant reaction was observed over several weeks,⁴⁹ in support of the kinetic inertness of the Cr(III) ion. Considering the reported routes to Crq₃, the method used by Li *et al.* involved reacting chromium nitrate and 8-hydroxyquinoline in the presence of gadolinium(III) nitrate.⁴⁵ However, since the presence of trace quantities of Gd(III) may have adverse effects on the spectral and magnetic properties of Crq₃, we have opted for adaption of another literature method involving reaction of chromium(III) and 8-hydroxyquinoline in the presence of urea and

ammonium chloride/acetic acid buffer.^{38,50} The product has been characterized by elemental analysis, mass spectrometry, thermogravimetry, FTIR, ¹H NMR spectroscopy, and X-ray powder diffraction. Additional information on both geometric and electronic structure has come from density functional theory (DFT) calculations, and UV/Visible absorption and diffuse reflectance spectra. Preliminary studies on its luminescence have also been made. These are complemented by detailed cyclic voltammetry studies on Crq₃, Alq₃ and the ligand 8Hq. Comparison of CV and electronic spectral data with results from DFT calculations provides details on both structure and electronic properties, which are used as a framework to assess the potential of this system for optoelectronic applications.

2. Experimental

2.1. Reagents

Chromium nitrate hexahydrate (Cr(NO₃)₃·6·H₂O) was purchased from Merck, and 8-hydroxyquinoline was obtained from Aldrich and used without further purification. Synthesis of the Alq₃ sample used has been described elsewhere.⁵¹ All solvents were of the highest purity commercially available and, where appropriate, were further purified by literature procedures.

2.2. Synthesis of Crq₃ by the Urea Method

This is based on a literature procedure.^{38,50} The product was recrystallized in a water/methanol mixture (10:90 %) by slow evaporation at room temperature. A brown powder was obtained after one week. Yield: 80% (based on Cr ions). The precipitate is soluble in common organic solvents such as acetone, benzene, chloroform or alcohol. Elemental analysis (%): C 65.08 (expected for CrC₂₇H₁₈N₃O₃: 66.94; expected for CrC₂₇H₁₈N₃O₃·CH₃OH 65.11); H, 4.35 (expected for CrC₂₇H₁₈N₃O₃: 3.75; expected for CrC₂₇H₁₈N₃O₃·CH₃OH 4.29); N 8.02 (expected for CrC₂₇H₁₈N₃O₃: 8.67; expected for CrC₂₇H₁₈N₃O₃·CH₃OH 8.14) is fully consistent with the product being a methanol solvate of Crq₃.

2.3 Equipment and methods

Mass spectra were measured using a MALDI-TOF, Voyager-DE™ PRO Workstation, with positive reflector mode acquisition.

Carbon, hydrogen and nitrogen elemental analyses were performed in duplicate at the *Servicio de Análisis Instrumental – Unidad de Análisis Elemental*, CACTI Vigo, Universidad de Vigo, Spain.

Thermogravimetry was performed using a Netzsch thermal analyzer, TG 209 F3, over the range 30-900 °C in a dynamic N₂ atmosphere with a heating rate of 10 °C.min⁻¹. The chromium content was determined by igniting a known weight of the dried precipitate and weighing the chromium(III) oxide.

The Fourier Transform-Infrared Spectroscopy (FTIR) was carried out over the range 4000–400 cm⁻¹ with resolution of 1 cm⁻¹ on samples in KBr pellets on a Nicolet FT-IR 6700 spectrophotometer, or using an ATR Smart Orbit ATR Diamond Attenuated Total Reflectance (ATR) accessory with a Thermo Nicolet 380 FTIR spectrometer.

The ¹H NMR spectra were obtained on a Varian Unity-500 NMR spectrometer (at 499.843 MHz), using sw=41972.72 Hz, tof=67.38 Hz, at=1.5 s, d1=0.2 s. The methyl signal of tert-butyl alcohol and the signal of DMSO were used as internal references for ¹H, in D₂O (δ 1.3 ppm relative to TMS) and in DMSO (δ 2.5 ppm relative to TMS) solutions, respectively.

X-ray powder diffractograms were obtained using an ENRAF-NONIUS FR590 powder diffractometer equipped with an INEL120 detector (Debye-Scherrer geometry) using CuKα radiation. The powder was used to fill a glass capillary, which was slowly rotating upon data collection. Calibration was performed using silicon as an external calibrant.

Cyclic voltammetry (CV) measurements were performed on a computer-controlled μ-Autolab type I potentiostat-galvanostat with GPES software (Metrohm-Autolab, Utrecht, Netherlands). The experiments were carried out in acetonitrile (ACN) containing 0.1 M tetra-*n*-butylammonium perfluorate (TBAP) as supporting electrolyte. A three-electrode system was used and consisted of a glassy carbon working electrode (1 mm diameter), a platinum wire counter electrode, and an Ag/AgCl reference electrode. Peak currents were measured from extrapolation of the baseline just before the peaks in the cyclic voltammograms.

UV–Visible absorption spectra in solution were measured over the range 200–800 nm on a Shimadzu UV-2010 double-beam spectrometer, with samples in 1 cm quartz cuvettes. Diffuse reflectance (DRS-UV–vis) spectra of solid samples were recorded over the range 300–800 nm on a Shimadzu UV-2450 double-beam spectrometer with an integrating sphere, using barium sulfate as reference material.

Photoluminescence (PL) excitation and emission data were collected on samples in solution in 1 cm quartz cuvettes with a Spex Fluorolog 3-22 spectrophotometer, using a 300 W xenon arc lamp as excitation source.

2.4 DFT Computational Details

The molecular structures of the open shell d^3 (quartet state) *meridional* and *facial* $[\text{Cr}(\text{Hq})_3]$ isomers were optimized using the GAMESS-US code⁵² at the DFT level using the B3LYP (Becke three-parameter Lee-Yang-Parr)^{53,54} exchange correlation functional. The geometries were optimized without symmetry constraints in the case of the *meridional* structure (C_1 point group) and constraining the symmetry to the C_3 point group in the case of the *facial* isomer. The calculations were performed using both the restricted open-shell (RO-B3LYP) and the unrestricted (U-B3LYP) formalisms. In the case of the U-B3LYP calculations, spin-contamination was assessed by a comparison of the expected $S(S + 1)$ for the assigned spin state and the actual value of $\langle S^2 \rangle$. The Stuttgart relativistic small core (RSC) 1997 valence and effective core potential (ECP) functions⁵⁵ were used for the metal and the 6-311G(d,p) basis sets were used for the expansion of the Kohn-Sham orbitals of the ligand atoms. The bulk solvent (DMSO or acetonitrile) effects were taken into account through the polarizable continuum model (PCM) of Tomasi and co-workers.^{56,57} Default van der Waals radii were used for all atoms except chromium, for which 2.36 Å was used. The Hessian was calculated for the resultant stationary points, and the geometries were characterized as true minima (i.e., no imaginary frequencies). The gradient threshold for geometry optimization was taken as 10^{-5} Hartree Bohr⁻¹. The geometries of the cation $[\text{Cr}(\text{Hq})_3]^+$ (d^2 configuration, triplet state) and of the anion $[\text{Cr}(\text{Hq})_3]^-$ (d^4 configuration) of the *meridional* isomer were also optimized using the same methods as for the neutral molecules. The ionization energy (Ip) and the electron affinity (Ea) were calculated as the difference between the ground state energies of the corresponding charge states and the neutral molecule, $\text{Ip} = E(+1) - E(0)$ and $\text{Ea} = E(0) - E(-1)$.⁵⁸ The calculations on the anion were done assuming a high

spin system (a system in which the additional electron occupies the LUMO orbital, therefore a quintet state). Additionally, the geometry of the anion and the neutral meridional isomer were also optimized using the 6-31+G(d) basis sets, which include diffuse functions to better represent the extra charge in the anion.

3. Results and discussion

3.1 Synthesis and characterization

As indicated in the Experimental Section, the compound was synthesized by adapting a literature method,^{38,50} involving reaction between chromium(III) (as its nitrate) and 8-hydroxyquinoline in an acetic acid/ammonium chloride/ammonium acetate buffered solution. The solid product was recrystallized from a water/methanol mixture (10:90 %) by slow evaporation at room temperature. Brown crystals appeared after several days (m.p. > 300 °C). As indicated in the Experimental section, the C, H, N elemental analysis is consistent with formation of the methanol solvate of Crq₃.

Confirmation of the formation of Crq₃ came from the MALDI-TOF mass spectrum (Fig. 1), where a clear molecular ion peak located at $m/z = 484.0408$ is observed, corresponding to Crq₃⁺ (theoretical value for CrC₂₇H₁₈N₃O₃⁺ from isotopic masses $m/z = 484.0753$).⁵⁹ Additional peaks located at $m/z = 507.0490$ and 523.0234 were observed, and may correspond to [M+Na]⁺ and [M+K]⁺, respectively. This contamination is probably due to the glass in contact with this type of sample, and is fairly common for organic compounds with an affinity for alkali metal cations.

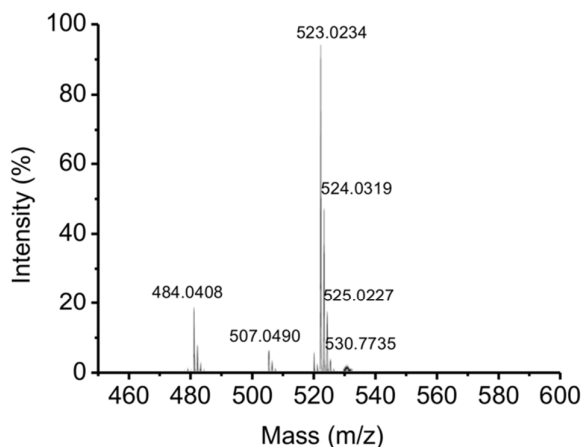


Fig. 1. MALDI-TOF mass spectrum of Crq₃.

The complex was also analysed by thermogravimetry (Fig. 2), which showed an initial small weight loss around 200 °C, a second step around 470 °C, and final weight losses between 500 and 700 °C. Previous studies on Crq_3 ^{36,46} and the corresponding cobalt(III) derivative⁶⁰ show that they tend to crystallize as alcohol adducts, with the solvent trapped in a “cage-like” cavity, and that the alcohol can be eliminated upon heating around 200 °C. From the thermogravimetric data, and C, H, N elemental analysis, we suggest that with our synthesis, the Crq_3 recrystallizes from 90% methanol-water with similarly trapped methanol molecules, and that these are lost in this first stage of heating. As we will see shortly, support for this comes from both FTIR and ¹H NMR spectra. Results in Table 1 show that the subsequent loss in weight is fully consistent with a stoichiometry involving three molecules of 8-hydroxyquinolate per atom of chromium. Ignition at ca. 470 °C for 1 h quantitatively converts the complex to chromium (III) oxide (Cr_2O_3) (Fig. 2). The residual mass confirms the presence of the oxide, and the thermal behaviour is similar to that of other metal quinolates.

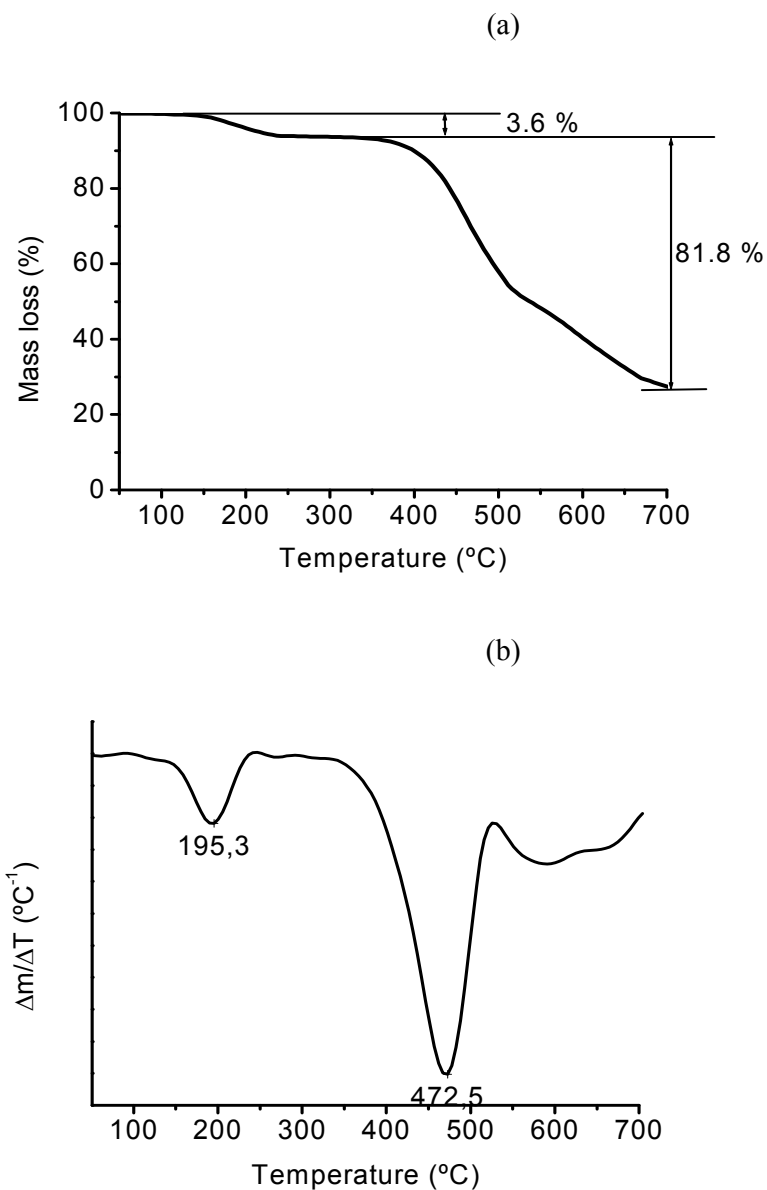


Fig. 2. (a) Thermogravimetric analysis of Crq_3 under nitrogen atmosphere; (b) differential thermogram.

Table 1-Thermogravimetric characteristics of Cr(III) complex.

Complex	Temp. range (°C)	Mass loss (%) (exp.)	Assignment	Residue
[$\text{C}_{27}\text{H}_{18}\text{N}_3\text{O}_3\text{Cr}$]. $0.5\text{CH}_3\text{OH}$	50-250	3.6	$0.5\text{CH}_3\text{OH}$	
	300-800	81.8	$\text{C}_{27}\text{H}_{18}\text{N}_3\text{O}_3$	$\frac{1}{2}\text{Cr}_2\text{O}_3$

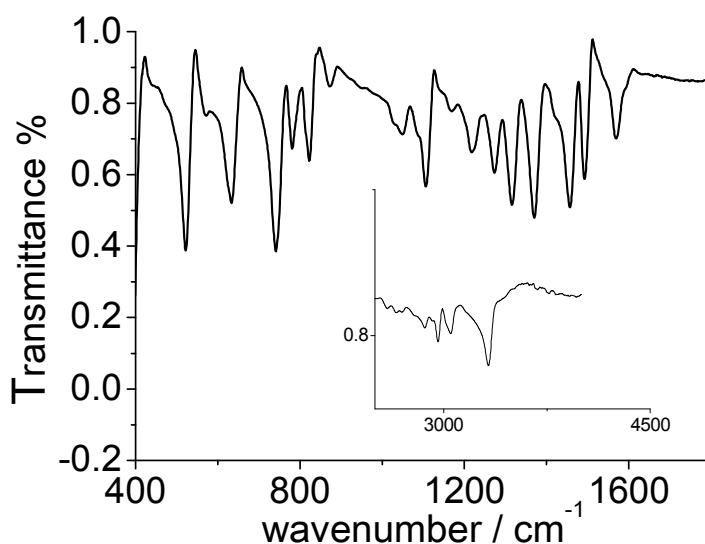
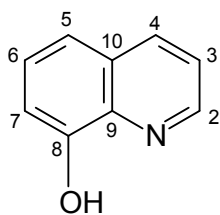


Fig. 3. FTIR spectrum of solid recrystallised from 90% methanol-water (Inset shows the 2500 – 4500 cm^{-1} region).

Solid samples of the product were analysed by FTIR spectroscopy, both as KBr disks and using attenuated total reflectance (ATR). The only significant difference observed between spectra obtained using these different sampling techniques was in the 3000-3600 cm^{-1} region, probably due to the presence of trace water in the KBr discs. The ATR spectrum is shown in Fig.3. All the characteristic bands observed in the IR spectra of the solid are presented as electronic supplementary information (ESI, Table S1), and are discussed in relation to the structure Crq_3 on the basis of literature data on various metal 8-hydroxyquinolates.^{37,61-65} The observation of an absorption around 3325 cm^{-1} and sharp bands at 2959 and 2866 cm^{-1} are attributed to methanol,⁶⁶ and are in complete agreement with the TG data of occluded solvent within the solid Crq_3 . These are markedly reduced in intensity on heating the sample to 200 °C, in agreement with methanol loss on heating.

Further information on the structure was obtained by ^1H NMR spectroscopy. In this discussion we will use the numbering of the ring positions of 8-hydroxyquinoline (8-Hq) indicated below.



Scheme 1. Structure of 8-hydroxyquinoline (8-Hq)

8-Hq is known to form extremely stable bidentate chelate complexes with most transition and main group metal cations. The ^1H NMR spectra of 8-Hq as well as the ^1H signals of the water soluble derivative 8-HqS, have previously been assigned in the literature.^{4,67}

For the determination of structural features of the complex Cr(III)/8-Hq in solution, we obtained the ^1H NMR spectra of both 8-Hq and the synthesized complex Cr(III)/8-Hq in DMSO- d_6 . Results are illustrated in Fig. 4 for the ^1H NMR spectra of 8-Hq and the complex Cr(III)/8-Hq. The complete ^1H NMR spectral parameters for 8-Hq and its complexes with Cr(III) are shown in Table 2. In addition, the spectrum of Crq₃ shows a broad band at 3.33 ppm attributed to methanol, in agreement with the thermogravimetry and FTIR results on the presence of this solvent.

The complexes are paramagnetic and, because of the rapid relaxation time caused by the paramagnetic properties of the Cr(III) metal ion, ^1H NMR signals of bound ligands (inner sphere) are observed to be dramatically broadened and shifted to high frequencies (Fig. 4 and Table 2). Based on the mass spectral and TG data, this is assumed to be the species with a 1:3 (metal:ligand) stoichiometry.

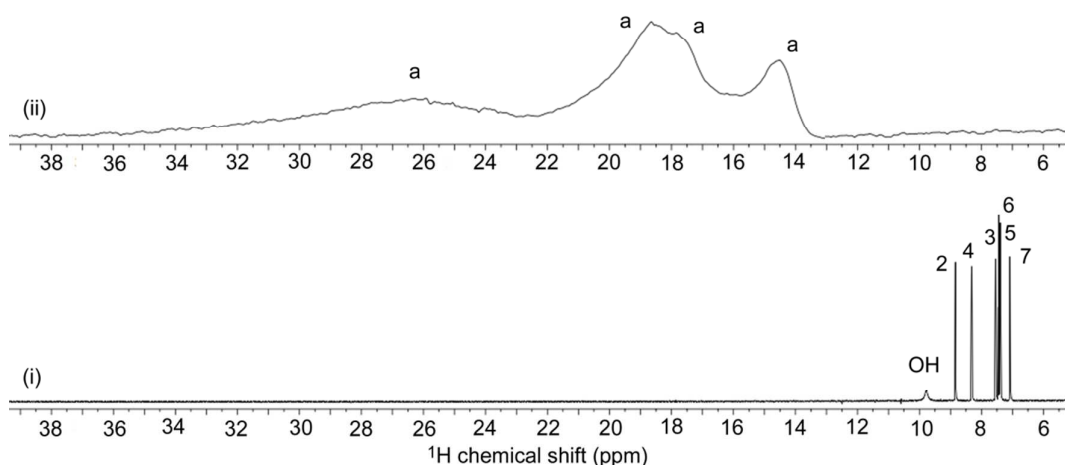


Fig. 4. ^1H NMR spectra (499.824 MHz) obtained from -30 to 50 ppm of $\text{DMSO-}d_6$ solutions of (i) 8-Hq 10 mmol dm^{-3} , and (ii) Cr(III)/8-Hq complex 10 mmol dm^{-3} .

Table 2. ^1H NMR parameters ^a for 8-Hq and its complexes with Cr(III) (298 K)

	H-2	H-3	H-4	H-5	H-6	H-7	OH	$J_{2,3}$	$J_{3,4}$	$J_{2,4}$	$J_{5,6}$	$J_{6,7}$	$J_{5,7}$
8-Hq ^b (δ)	8.85	7.55	8.32	7.39	7.44	7.08	9.77	4.2	8.3	1.7	7.5	7.5	1.4
Cr(III)/8-Hq ^c complex (δ)	25.0	/	18.6	/	17.6	/	14.4	- ^d	- ^e	- ^e	- ^e	- ^e	- ^e

^a δ values, in ppm, relative to Me_4Si , using the signal of DMSO as internal reference (δ 2.5 ppm); J values in Hz.

^b Solution of 8-Hq 10 mmol dm^{-3} in $\text{DMSO-}d_6$.

^c complex synthesized accordingly to the experimental procedure.

^d not detected.

^e not observed

Fig. 5 shows the comparison of the envelope signals for Crq_3 and Alq_3 , which also suggest that these complexes are homologous. Although the comparison of the ^1H NMR spectra of the paramagnetic complexes Crq_3 with the ^1H NMR spectra of the diamagnetic Alq_3 (Fig. 5) suggests a rough attribution, the large widths of the bound ligand resonances (metal ion inner sphere) of the Crq_3 complex precludes the complete assignment of the signals. However, the dramatic shifts observed are in accordance with

similar effects observed in previous studies on the acetylacetonate complex of Cr(III).^{68,69}

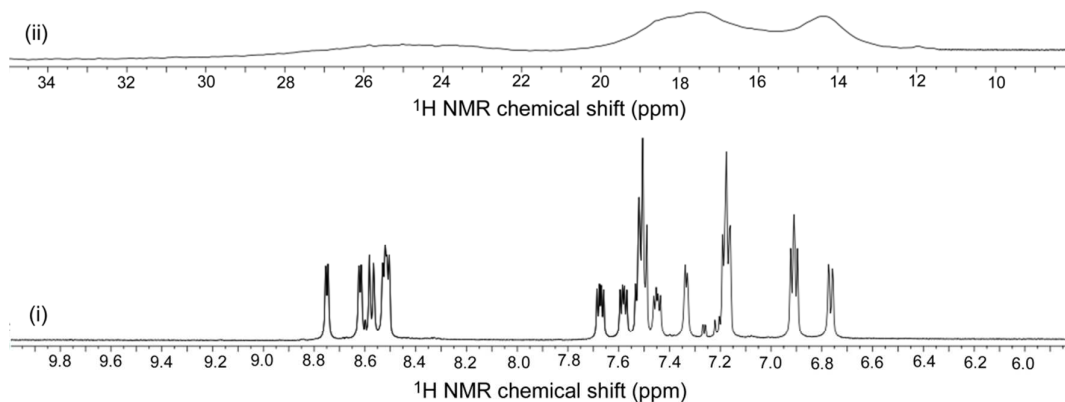


Fig. 5. ¹H NMR spectra (499.824 MHz) obtained from -30 to 50 ppm of (i) a D₂O solution of Al(III)/8-Hq (Alq₃) 10 mmol dm⁻³, and (ii) a DMSO-*d*₆ solution of Cr(III)/8-Hq complex 10 mmol dm⁻³.

Shifts as a result of ligand binding to paramagnetic metals may come either from through-space dipolar interactions (pseudo-contact), or from direct delocalization of unpaired electron spin-density from the metal (contact shift). The Cr(III) metal ion in the complex mainly produces a contact shift, which implies that the electron spin is partly delocalized between the 3d orbitals of the metal atom and the π orbitals of the ligand. Comparison with the behavior of chromium(III) acetylacetonate complexes⁶⁸ suggests that this involves ligand donation to the empty *e* orbitals of the metal. As we will see later, this is fully consistent with the DFT description of the electronic structure of the complex. The potential of Crq₃ as a paramagnetic NMR relaxation agent is discussed in the ESI.

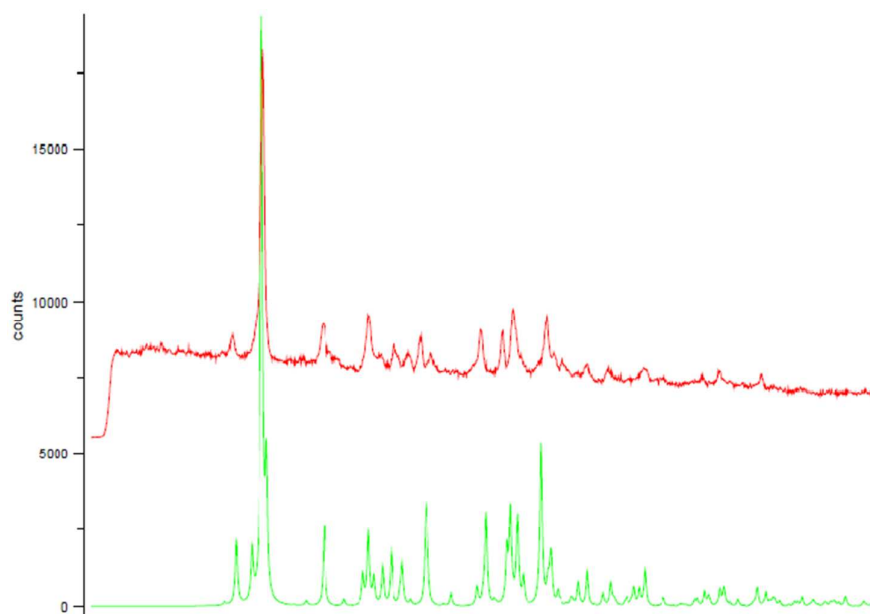


Fig. 6. X-ray powder diffractogram of the solid product. Top (in red) experimental powder diffraction. Bottom (in green) simulated powder diffractogram for Crq_3 methanol solvate.

Finally, the structure of the solid product was characterized by X-ray powder diffraction (Fig. 6). As seen by the great similarity between the experimental powder diffractogram and the simulated from the data reported by Li *et al.*⁷⁰ using PLATON,⁷¹ one can state that the main features of the supramolecular organization are common to both compounds. Most likely, our compound is a tris(8-quinolinato) chromium(III) methanol solvate almost isostructural to the already reported ethanol solvate.⁴⁶ Li *et al.* describe their complexes as having three 8-quinolinate ligands chelating to each Cr(III) ion in an octahedral geometry.⁷⁰ They observed short distances between the aromatic rings of neighboring complexes and presumed π - π interactions as one of the key factors regulating the supramolecular assembling. The ethanol solvent molecules are H-bonded to the metal complexes through the quinolate oxygen atom. The solvent molecules (four in each unit cell) occupy two large voids of 186 Å.

3.2 DFT studies

To help elucidate the coordination mode of Cr^{3+} with 8-Hq, the structures of the *meridional* and *facial* isomers of the complex were optimized at the DFT level and their

relative energies were determined. The results from the RO-B3LYP calculation indicate that the *meridional* isomer is more stable than the *facial* isomer by 10.56 kJ mol⁻¹ (10.71 kJ mol⁻¹ in the U-B3LYP calculation). The equilibrium geometry with minimum energy of the *mer*-[Crq₃] complex is shown in Fig. 7 and selected geometrical parameters are given in Table 3.

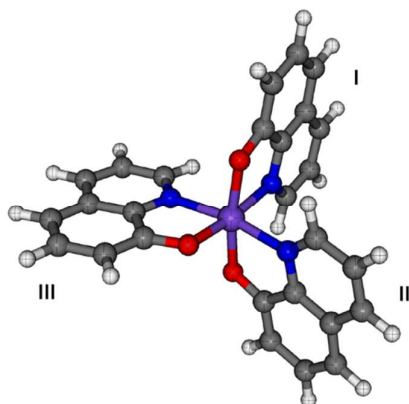


Fig. 7. Optimized RO-B3LYP geometry of the *mer*-[Crq₃] complex.

Table 3. Selected bond lengths (Å) and angles (degrees) calculated at the RO-B3LYP/6-311G(d,p) level in PCM (DMSO)^a for the *mer*-[Cr(Hq)₃] complex.

Bond lengths		Angles	
Cr-O _I	1.973	O _I -Cr-N _I	79.76
Cr-O _{II}	1.986	O _{II} -Cr-N _{II}	81.03
Cr-O _{III}	1.959	O _{III} -Cr-N _{III}	81.19
Cr-N _I	2.119	O _I -Cr-O _{II}	170.27
Cr-N _{II}	2.081	N _I -Cr-O _{III}	172.45
Cr-N _{III}	2.102	N _{II} -Cr-N _{III}	169.33

^a Polarizable Continuum Model^{56,57}

As expected due to the *trans* effect, the longest Cr-N bond is Cr-N_I, which is opposite to the shortest Cr-O bond (Cr-O_{III}).

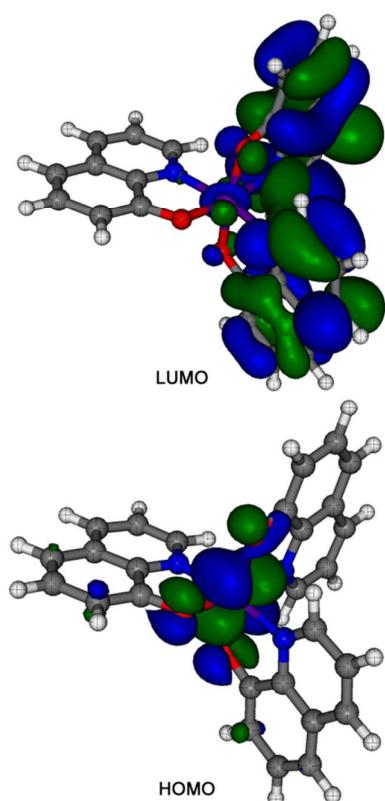


Fig. 8. Highest occupied (HOMO) and lowest unoccupied (LUMO) molecular orbitals for the *mer*-[Crq₃] complex calculated at the RO-B3LYP/6-311G(d,p) level of theory.

The LUMO in the complex is essentially localized on the ligands, but still has some charge on the metal (i.e. on the metal d_z^2 orbital). In contrast, the HOMO corresponds essentially to one of the t_2 metal orbitals (with some minor charge localized on the ligands) (Fig. 8). This has important implications on the oxidation and reduction processes which are relevant for charge injection in devices, as we will discuss later. The ionization energy of the complex was estimated using two different approaches. First, we considered the DFT counterpart of the Koopman's theorem which states that the first vertical ionization energy is equal to the negative of the energy of the highest occupied molecular orbital (HOMO). This is not entirely valid for the restricted open-shell orbitals; therefore we have considered the unrestricted calculation in this approach. In a second approach we have calculated the ionization energy as the difference between the ground state energies of the positive ion and the neutral molecule, $I_p = E(+1) - E(0)$. This was done either keeping the geometry fixed in the neutral ground

state geometry (vertical ionization energy), or at the optimized geometries of both the charged and neutral species (adiabatic ionization energy). In these calculations, the bulk effects of the solvent (DMSO or acetonitrile) were taken into account through the polarizable continuum model.^{56,57} Using the first approach, and considering DMSO as the solvent, we obtained a value of 5.47 eV for the ionization energy and using the second approach we obtained 5.63 and 5.95 eV for the adiabatic and vertical ionization energies, respectively. Changing the solvent from DMSO to acetonitrile had a negligible effect on the vertical ionization energy, which only increased to 5.96 eV.

The accurate computation of the electron affinity is more difficult because the correct calculation of the structure and energy of the anion is strongly dependent on the basis set used. Additionally, the negative of the lowest unoccupied molecular orbital (LUMO) energy in the neutral system is not a good estimate for the electron affinity.⁷² A rather better approximation is to use the negative of the energy of the additional occupied orbital in the anion. Using this approach we obtained a value of 2.45 eV for the U-B3LYP calculation of the anion with the 6-311G(d,p) basis set and 2.51 eV using the 6-31+G(d) basis set. Additional calculations using the $E_a = E(0) - E(-1)$ approach gave the value of 2.23 eV for the adiabatic electron affinity calculated at the U-B3LYP level with the 6-31+G(d) basis set.

3.3 Cyclic voltammetry

Cyclic voltammetry has been performed on Crq₃, Alq₃ and, for comparison, the free ligand 8-Hq in acetonitrile solutions using a three-electrode system consisting of a glassy carbon working electrode, a platinum wire counter electrode, and an Ag/AgCl reference electrode. The results are shown in Figures 9 and 10. The quinolate solutions were prepared and stored in the fridge in between use. The same voltammetric profiles were recorded when using the prepared quinolate solutions during more than 2 months, which indicates the high stability of the compounds in acetonitrile.

The compound Crq₃ presents 4 oxidation peaks in the positive region in the first scan, and two corresponding, less intense reduction waves and in the negative region two pairs of reversible peaks. The oxidation peaks are located at 0.85, 1.18, 1.42 and 1.60 V vs. Ag/AgCl with peak currents of 350, 150, 150, and 380 $\mu\text{A cm}^{-2}$ for peaks 1, 2, 3 and 4, respectively. The corresponding reduction waves, which, unlike the oxidation ones,

are of constant height on cycling the potential, are situated at 0.84 and 1.53 V vs. Ag/AgCl with very small current densities of 88 and 40 $\mu\text{A cm}^{-2}$, respectively.

Oxidation peak 1 merges with peak 2, and shifts towards more positive potentials upon cycling, from 0.85 to 1.13 V, at which potential it stabilizes. Peaks 3 and 4 merge during the second scan and form a broader peak with similar current intensity at 1.50 V. This merged peak decreases drastically in scan 3, and then splits to form peaks 3 and 4 again during further CV scans. After 4 scans, the CV profile contains 3 oxidation peaks at 1.13, 1.41 and 1.53 V vs. Ag/AgCl, with peak currents of 330, 120 and 150 $\mu\text{A cm}^{-2}$, respectively.

In the negative region, two pairs of reversible peaks appear with midpoint potentials of -0.76 and -1.40 V vs Ag/AgCl. The oxidation peaks remain constant with potential cycling, while the reduction peak current 1' decreases to half the value in scan 2, from 1260 to 580 $\mu\text{A cm}^{-2}$, and then remains constant. Reduction peak 2' becomes better defined in the second and following CV-s, and the peak current increases from 130 to 230 $\mu\text{A cm}^{-2}$.

The compound Alq₃, in the first CV scan, presents two irreversible oxidation peaks in the positive region, which, as in the case of Crq₃, then merge into one peak with considerably reduced currents, and shows one pair of peaks in the negative region, which remained unchanged during cycling. The oxidation peaks 1 and 2 appear at the potentials $E_{\text{ox}1} = 1.11$ V and $E_{\text{ox}2} = 1.31$ V vs. Ag/AgCl, with peak currents $j_{\text{ox}1} = 550$ and $j_{\text{ox}2} = 570$ $\mu\text{A cm}^{-2}$, respectively. During cycling, these two peaks merge into one at 1.18 V, with a lower current of 50 $\mu\text{A cm}^{-2}$. The fact that, after polishing the electrode to have a clean electrode surface, the two peaks in scan 1 reappear with similar current densities, indicates that oxidation products or by-products may cover the electrode, leading to the decrease in current in second and subsequent cycles. In the negative region, a quasi-reversible reaction occurs, with midpoint potential of -0.70 V, with $j_{\text{red}1'} = 1300$ $\mu\text{A cm}^{-2}$ and $j_{\text{ox}1'} = 840$ $\mu\text{A cm}^{-2}$.

For comparison, studies were carried out on the free ligand, 8-Hq, which presents two oxidation peaks in the positive region in the first cycle with a small reduction wave, and one reduction and two oxidation peaks in the negative region. The oxidation peaks in the positive region are situated at 0.73 and 1.16 V vs Ag/AgCl, with peak currents of 500 and 150 $\mu\text{A cm}^{-2}$. After 5 cycles, these oxidation peaks are shifted towards more positive potentials of 0.93 and 1.31 V vs Ag/AgCl, with lower constant currents of 350

and $130 \mu\text{A cm}^{-2}$. In the negative region, there is one main reduction peak during the first scan at -0.98 V , height $1470 \mu\text{A cm}^{-2}$, and a small shoulder at -0.77 V . Upon cycling, the shoulder at -0.77 V becomes bigger, a new small peak appears at -1.42 V , peak current $120 \mu\text{A cm}^{-2}$, together with a new, less evident reduction wave at -1.90 V vs Ag/AgCl. The main reduction peak decreases slightly from 1470 to $1360 \mu\text{A cm}^{-2}$, from first to last cycle.

The oxidation peaks 1' and 2' are situated at -0.48 and -0.69 V , with peak currents of 790 and $820 \mu\text{A cm}^{-2}$, which slightly increase with potential cycling to 900 and $920 \mu\text{A cm}^{-2}$.

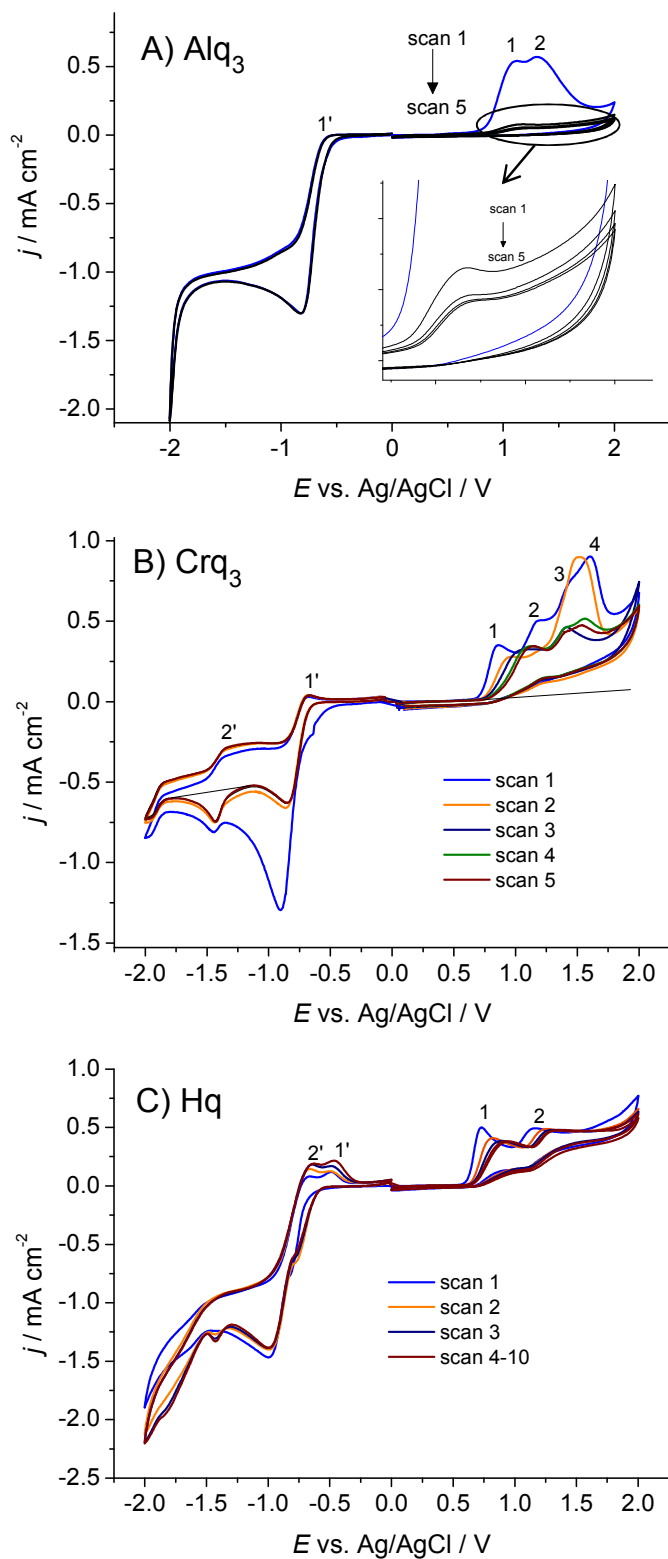


Fig. 9_ Cyclic voltammograms recorded at A) Alq₃, B) Crq₃, and C) 8-Hq in 0.1 M TBAP in ACN at $\nu = 50 \text{ mV s}^{-1}$.

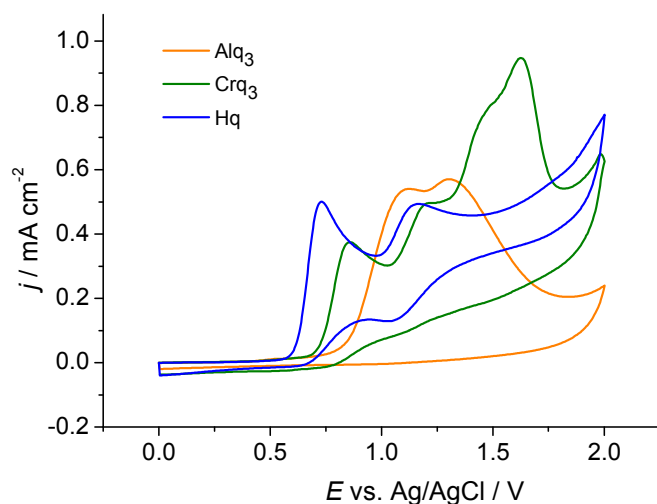


Fig. 10. Cyclic voltammograms (first scan) recorded in the positive potential region at Alq₃, Crq₃, and 8-Hq in 0.1 M TBAP in ACN at $\nu = 50 \text{ mV s}^{-1}$.

Full details are summarized in Tables 4 and 5.

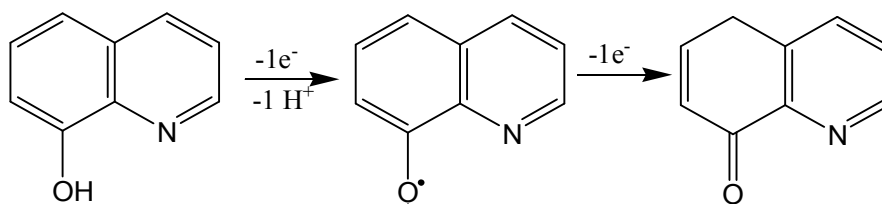
Table 4. Oxidation potentials extracted from the CVs for the compounds Alq₃, Crq₃, and 8-Hq

Compound	Scan n°	$E / \text{V vs Ag/AgCl}$				$j / \mu\text{A cm}^{-2}$			
		Ox1	Ox2	Ox3	Ox4	Ox1	Ox2	Ox3	Ox4
Alq ₃	1	1.11	1.31	-	-	550	570	-	-
	10	1.18		-	-	50		-	-
Crq ₃	1	0.85	1.18	1.42	1.60	350	150	150	380
	10	1.13		1.41	1.53	330		120	150
8-Hq	1	0.73	1.16	-	-	500	150	-	-
	10	0.93	1.31	-	-	350	130	-	-

The first two peaks observed in the CVs of Alq₃ are related to 8-Hq. Peak number 1 is irreversible, and is attributed to the formation of $-\text{O}^\bullet$ radicals,⁷³ and the second one, quasi-reversible, to the formation of a quinoid-like structure, as presented in Scheme 2. With Alq₃, the oxidation potentials are shifted to more positive values those of 8-Hq,

since the oxygen atom of the ligand covalently binds the central metal ion, which makes its oxidation more difficult. As has previously been reported, with Alq₃, the oxidations are irreversible.⁷⁴ In the case of Crq₃, the first peak is at 0.85 V, while further peaks are seen at 1.18, 1.42 and 1.60 V. The oxidation is more reversible in this case than with Alq₃, in agreement with our prediction. With potential cycling, for both complexes, peaks 1 and 2 merge into one peak, at 1.18 and 1.13 V vs. Ag/AgCl, respectively, having different current densities, markedly lower for Alq₃ (50 $\mu\text{A cm}^{-2}$) than for Crq₃ (330 $\mu\text{A cm}^{-2}$). The decrease in the oxidation peak currents in the positive region after the first 2 cycles is, in both cases, related to the passivation of the electrode by decomposition products of the quinolates. Nevertheless, this decrease is significantly greater in the case of Alq₃, which clearly indicates that Crq₃ does not decompose as much as Alq₃.

The peaks 3 and 4 for Crq₃ are attributed to formation of higher metal oxidation states.



Scheme 2. Oxidation mechanism of 8-Hq

Table 5. First oxidation/reduction potentials, and corresponding I_p and E_a , and gap energy E_g extracted from the CVs for the compounds Alq₃ and Crq₃.

	E_{ox} / V	$-I_p (E_{\text{HOMO}}) / \text{eV}$	$E_{\text{red}} / \text{V}$	$-E_a (E_{\text{LUMO}}) / \text{eV}$	E_g / eV
Alq ₃	1.11	-5.51	> -2.0*	> -2.40	> 3.11
Crq ₃	0.85	-5.25	-1.37	-3.03	2.22

* E_{red} of Al³⁺ probably occurs at more negative potentials, out of the potential range of the electrode.

The HOMO and LUMO energies, together with the HOMO-LUMO separation (E_g) were calculated from the oxidation and reduction potentials using the expressions given in equations (1) and (2). For Alq₃, the HOMO energy is in excellent agreement with the

literature value of -5.65 eV.⁷⁵ The LUMO energy cannot be measured directly because it is outside the potential range of the GCE in organic media, but is fully consistent with literature values of -2.90 V⁷⁵ and -3.0 V.¹⁶

For Crq₃, the HOMO energy is close to the value -5.47 eV, calculated considering the DFT counterpart of Koopman's theorem, with solvent included. The value is also in reasonable agreement with that calculated for the adiabatic ionization energy from the difference in ground state energies between the positive form and the neutral molecule, at their optimized geometries (-5.63 eV). This provides strong support to the idea from the DFT calculations that the HOMO is mainly localized on one of the metal d orbitals. The agreement between the LUMO energy obtained by CV (-3.03 eV) and that obtained by DFT (for example, -2.51 eV using the 6-31+G(d) basis set) was less good. However, we discussed earlier the difficulties in the accurate calculation of electron affinity in these systems. Similar underestimation of LUMO energies in DFT calculations have previously been reported for Alq₃.⁷⁵

3.3 UV/Visible absorption and luminescence spectral studies

The UV/Visible absorption spectra for complex Crq₃ in two solvents, dichloromethane and dimethylsulfoxide, are essentially identical, and are shown in Fig. 11. Two intense absorption bands at approximately 270 and 420 nm dominate the spectrum. These are reminiscent of the corresponding bands in the *mer* isomer of Alq₃⁷⁶ and, based on this can be assigned to the ligand centred electronic transitions. In addition to these intense bands, there is a weak absorption band at 324 nm, which may be part of a vibronic progression associated with the deformation mode.⁷⁶ In the region between 500–700 nm, there is a broad, low intensity shoulder at ca. 558 nm. Although not observed in a recent report on this compound,⁴³ probably because the solutions used were too dilute, this band was seen in early studies on Crq₃,³⁶ and can be attributed to a d–d transition of the chromium ion. These bands have low molar absorption coefficients, ϵ , because they are Laporte “forbidden” transitions. The observation of this band is in complete agreement with the DFT results indicating that the HOMO is mainly localized on the metal t₂ orbital. Based on literature data on related chromium(III) complexes²⁷ the 558 nm band is attributed to the ⁴A₂ → ⁴T₂ transition. We note the absence of any n → π* band, in agreement with the formation of the metal–nitrogen bond, with the quinolate

complex stabilizing the electron pair on the nitrogen atom.⁷⁷ The energy of this shoulder (2.22 eV), which corresponds to the HOMO-LUMO gap, is identical to that determined by CV. Whilst the perfect agreement is, possibly, fortuitous, it fully supports the assignment of the HOMO to a metal based level in this system. An earlier report⁴³ of a band gap of 2.54 eV for Crq₃ in films corresponds to the $\pi \rightarrow \pi^*$ transition from the HOMO-1 level localized on one of the quinolate rings to the LUMO.

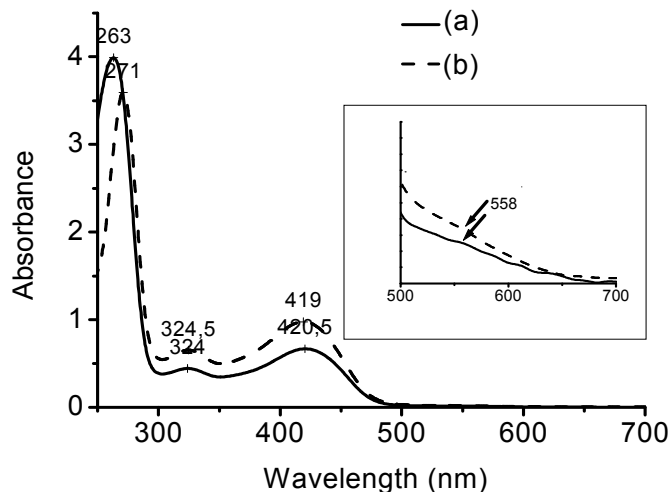


Fig. 11. UV/Visible absorption spectra of Crq₃ in (a) dichloromethane and (b) dimethylsulfoxide. (Insert: region between 500-700 nm).

The solid-state diffuse reflectance spectrum for the complex (Fig. 12), presents similar bands to those observed in solution, albeit with a small blue shift. The lowest energy band may be slightly shifted from 558 to 543 nm. The diffuse reflectance UV-Visible spectrum of the starting chromium(III) salt, Cr(NO₃)₃.6H₂O, was also run for comparison. There is a blue shift in the $^4A_2 \rightarrow ^4T_2$ transition of 34 nm (about 1085 cm⁻¹) on going from the hydrated chromium nitrate salt to Crq₃, indicating a stronger ligand field due to the 8-hydroxyquinolate in the latter case.

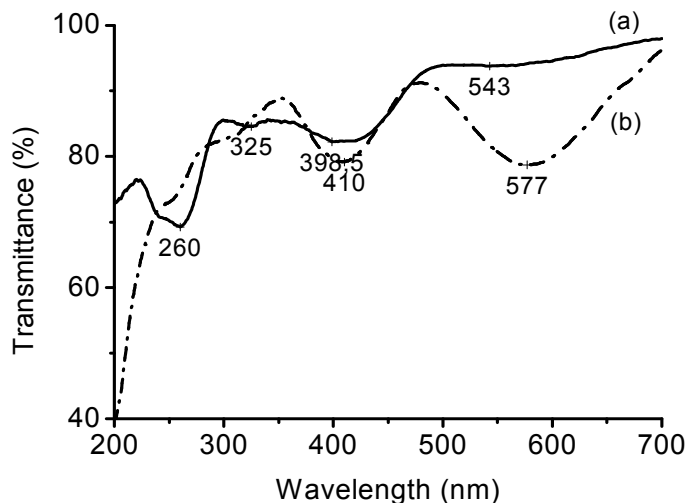


Fig. 12. Diffuse Reflectance UV/Visible spectra of (a) Crq_3 and (b) $\text{Cr}(\text{NO}_3)_3 \cdot 6\text{H}_2\text{O}$, in pressed BaSO_4 disks.

Attempts were made to obtain the emission spectrum of this complex in both solution and the solid state. Upon excitation at 430 nm, a very weak emission was observed around 670 nm (quantum yield ≤ 0.008). The spectrum is given in the ESI. The behaviour contrasts with the intense green, ligand-based emission in Alq_3 ($\lambda_{\text{emission}}$ 535 nm, quantum yield 0.116 in dimethylformamide),^{13,78} and related compounds of $\text{Al}(\text{III})$,^{47,79} $\text{Ga}(\text{III})$ ⁴⁸ and $\text{Zn}(\text{II})$,⁴ again supporting differences in the nature of the lowest energy excited state. With the compound formed between 8-hydroxyquinoline-5-sulfonate and vanadium(V) oxoion, the ligand based green emission is weaker than with the free ligand. This is suggested to be due to the presence of low-lying ligand-to-metal charge-transfer state(s).⁸⁰ However, the weakness of the emission with Crq_3 , is attributed to it involving a metal based transition. Further studies are in progress to fully characterize this at room temperature and low temperature.

4. Conclusions

In summary, we have synthesized a *mer*-tris(8-hydroxyquinolato)-chromium(III) complex, and have fully characterized it by elemental analysis, mass spectrometry, thermogravimetry, FTIR, ^1H NMR spectroscopy, X-ray powder diffraction and DFT calculations. The compound forms as a methanol solvate. However, methanol can be removed by heating. Cyclic voltammetry, DFT calculations and UV/Visible absorption and diffuse reflectance spectra allow determination of HOMO and LUMO energies, and are fully consistent with the HOMO being localized on the metal atom. The significantly higher and constant oxidation currents recorded for Crq_3 upon repeated cycling, compared with the commonly used Alq_3 , suggests the potential of this system as an electron transport/hole blocking layer in optoelectronic devices. Future experiments are planned to test this.

Acknowledgements

We are grateful to Professor M. E. S. Eusébio for access to the FTIR facilities. The authors thank the financial support of the “The Coimbra Chemistry Centre” from the Fundação para a Ciência e a Tecnologia (FCT), Portuguese Agency for Scientific Research, through the project PEst-OE/QUI/UI0313/2014 and Rede Nacional de RMN (REDE/1517/RMN/2005), the Portuguese NMR Network, for spectrometer facilities.

NMR data was collected at the UC-NMR facility which is supported in part by FEDER – European Regional Development Fund through the COMPETE Programme (Operational Programme for Competitiveness) and by National Funds through FCT – Fundação para a Ciência e a Tecnologia (Portuguese Foundation for Science and Technology) through grants REEQ/481/QUI/2006, RECI/QEQ-QFI/0168/2012, CENTRO-07-CT62-FEDER-002012, and Rede Nacional de Ressonância Magnética Nuclear (RNRMN). M.S., L.L.G.J., S.M.F. and M.M.B. also thank the FCT for the postdoctoral grants SFRH/BPD/34372/2007, SFRH/BPD/97026/2013, SFRH/BPD/34703/2007 and SFRH/BPD/72656/2010. In addition, we thank the Laboratory for Advanced Computing at University of Coimbra for providing computing resources that have contributed to the research results reported within this paper (URL <http://www.lca.uc.pt>).

References

- 1 J. J. Fox, *J. Chem. Soc.* 1910, **97**, 1119–1125.
- 2 K. Soroka, R. S. Vithanage, D. A. Philips, B. Walker and P. K. Dasgupta, *Anal. Chem.* 1987, **59**, 629–636.
- 3 M. Roysen, A. Durandin, V. G. Young Jr., N. E. Geacintov and J. W. Canary, *J. Am. Chem. Soc.* 2006, **128**, 3854–3855.
- 4 M. L. Ramos, L. L. G. Justino, A. Branco, C. M. G. Duarte, P. E. Abreu, S. M. Fonseca and H. D. Burrows, *Dalton Trans.* 2011, **40**, 11732–11741.
- 5 M. A. Palacios, Z. Wang, V. A. Montes, G. V. Zyranov and P. Anzenbacher, Jr., *J. Am. Chem. Soc.* 2008, **130**, 10307–10314.
- 6 J. P. Phillips, *Chem. Rev.* 1956, **56**, 271–297.
- 7 G. H. Jeffery, J. Bassett, J. Mendham and R. C. Denney, *Vogel's Textbook of Quantitative Chemical Analysis*, Longman, Harlow, UK, 5th edn., 1989, pp.441–442.
- 8 V. Ravindran, M. R. Stevens, B. N. Badriyha and M. Pirbazari, *AIChE J.*, 1999, **45**, 1135–1146.
- 9 M. J. Hannon, *Pure Appl. Chem.*, 2007, **79**, 2243–2261.
- 10 A. R. Timerbaev, *Metallomics*, 2009, **1**, 193–198.
- 11 G. Bandoli, A. Dolmella, F. Tisato, M. Porchia and F. Refosco, *Coord. Chem. Rev.*, 2009, **253**, 56–77.
- 12 M. Albrecht, M. Fiege and O. Osetska, *Coord. Chem. Rev.* 2008, **252**, 812–824.
- 13 C. W. Tang and S. A. VanSlyke, *Appl. Phys. Lett.* 1987, **51**, 913–915.
- 14 K. T. Kamtekar, A. P. Monkman and M. R. Bryce, *Adv. Mater.* 2010, **22**, 572–582.
- 15 S. Aihara, Y. Hirano, T. Tajima, K. Tanioka, M. Abe, N. Saito, N. Kamata and D. Terunuma, *Appl. Phys. Letts.* 2003, **82**, 511–513.
- 16 J. D. Anderson, E. M. McDonald, M. L. Anderson, E. L. Ritchie, H. K. Hall, T. Hopkins, E. A. Mash, J. Wang, A. Padias, S. Thayumanavan, S. Barlow, S. R. Marder, G. E. Jabbour, S. Shaheen, B. Kippelen, N. Peyghambarian, R. M. Wightman and N. R. Armstrong, *J. Am. Chem. Soc.* 1998, **120**, 9646–9655.
- 17 J. L. Bredas, R. Silbey, D. S. Boudreux and R. R. Chance, *J. Am. Chem. Soc.* 1983, **105**, 6555–6559.
- 18 A. P. Kulkarni, C. J. Tonzola, A. Babel, S. A. Jenekhe, *Chem. Mater.* 2004, **16**, 4556–4573.

- 19 P. E. Burrows, Z. Shen, V. Bulovic, D. M. McCarty, S. R. Forrest, J. A. Cronin and M. E. Thompson, *J. Appl. Phys.* 1996, **79**, 7991–8006.
- 20 S. Scholz, C. Corten, K. Walzer, D. Kuckling and K. Leo, *Org. Electron.* 2007, **8**, 709–717.
- 21 S. Schmidbauer, A. Hohenleutner and B. König, *Adv. Mater.* 2013, **25**, 2114–2129.
- 22 S. Scholz, B. Lüssem and K. Leo, *Appl. Phys. Lett.* 2009, **95**, 183309-1–183309-3.
- 23 H. D. Burrows, D. Costa, M. L. Ramos, M. da G. Miguel, M. H. Teixeira, A. A. C. C. Pais, A. J. M. Valente, M. Bastos and G. Bai, *Phys.Chem.Chem.Phys.* 2012, **14**, 7950–7953.
- 24 F. A. Cotton and G. Wilkinson, *Advanced Inorganic Chemistry*, 5th edn., Wiley, New York, 1988, pp.679–680
- 25 L. Helm and L. A. E. Merbach, *Chem. Rev.* 2005, **105**, 1923–1959.
- 26 R. F. P. Pereira, M. J. Tapia, A. J. M. Valente, H. D. Burrows, *Langmuir* 2012, **28**, 168–177.
- 27 K. DeArmond and L. E. Forster, *Spectrochim. Acta* 1963, **19**, 1393–1401
- 28 K. DeArmond and L. E. Forster, *Spectrochim. Acta*, 1963, 19, 1403-1406.
- 29 A. D. Kirk and G. B. Porter, *J. Phys. Chem.* 1980, **84**, 887–891.
- 30 L. E. Forster, *Coord. Chem. Rev.* 2004, **248**, 261–272.
- 31 P. S. Wagenknecht and P. C. Ford, *Coord. Chem. Rev.* 2011, **255**, 591–616).
- 32 M. Schnuriger, E. Tague and M. M. Richter, *Inorg. Chim. Acta* 2011, **379**, 158–162
- 33 R. B. Lauffer, *Chem. Rev.* 1987, **87**, 901–927.
- 34 S. Aime, C. Cabella, S. Collumbatto, S. G. Crich, E. Gianolio and F. Maggioni, *J. Magn. Reson. Imaging* 2002, **16**, 394–406.
- 35 E. Taylor-Austin, *Analyst*, 1938, **63**, 710–712.
- 36 F. Umland and K. Adam, *Z. Anorg. Chem.* 1965, **341**, 308–323.
- 37 K. Nakamoto and N. Ohkahu, *Inorg. Chem.* 1971, **10**, 798–805.
- 38 J. R. Rao and M. N. Sastri, *Fresenius Z. Anal. Chem.* 1972, **259**, 286–288.
- 39 V. Gemmer-Čolos and R. Neeb, *Fresenius Z. Anal. Chem.* 1980, **97**, 97–100.
40. E. K. Paleologos, C. D. Stalikas, S. M. Tzouwara and M. J. Karayannis, *Anal. Chim. Acta* 2001, **436**, 49-57.
41. W. G. Hanna and M. M. Moawad, *J. Coord. Chem.* 2002, **55**, 43-60.
42. M. S. Aksoy, *Asian J. Chem.* 2009, **21**, 5189-5198.
43. L. M. A. Monzon, F. Burke and J. M. D. Coey, *J. Phys. Chem. C* 2011, **115**, 9182-9192.

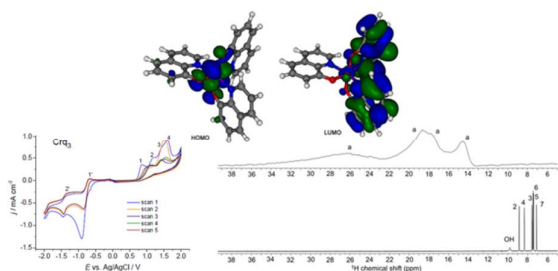
44. X. Xie, X. J. Xiang, J. Liu, X. Y. Ren, H. M. Wang and X. M. Liu, *Inorg. Chim. Acta* 2012, **383**, 132-136.
- 45 B. Li, J. Zhang, X. Zhang, J. Tian and G. Huang, *Inorg. Chim. Acta* 2011, **366**, 241–246.
- 46 K. Folting, M. M. Cox, J. W. Moore and L. L. Merritt, *Chem. Commun.* 1968, 1170–1171.
- 47 M. L. Ramos, L. L. G. Justino, A. I. N. Salvador, A. R. E. de Sousa, P. E. Abreu, S. M. Fonseca and H. D. Burrows, *Dalton Trans.* 2012, **41**, 12478–12489.
- 48 M. L. Ramos, A. R. E. de Sousa, L. L. G. Justino, S. M. Fonseca, C. F. G. C. Geraldes and H. D. Burrows, *Dalton Trans.* 2013, **40**, 3682–3694.
- 49 A. R. Freitas, *Undergraduate Research Project Report*, University of Coimbra, 2012.
- 50 M. Kitano, K. Yamagata and Y. Yamazaki, *J. Chem. Soc. Japan, Pure Chem.* 1969, **Sect. 90**, 190, cited in ref. 38.
- 51 H. D. Burrows, M. Fernandes, J. Seixas de Melo, A. P. Monkman and S. Navaratnam, *J. Am. Chem. Soc.*, 2003, **125**, 15310-15311.
- 52 M. W. Schmidt, K. K. Baldrige, J. A. Boatz, S. T. Elbert, M. S. Gordon, J. H. Jensen, S. Koseki, N. Matsunaga, K. A. Nguyen, S. J. Su, T. L. Windus, M. Dupuis and J. A. Montgomery, *J. Comput. Chem.* 1993, **14**, 1347–1363.
- 53 A. D. Becke, *J. Chem. Phys.* 1993, **98**, 5648–5652.
- 54 C. Lee, W. Yang and R. G. Parr, *Phys. Rev. B: Condens. Matter* 1988, **37**, 785–789.
- 55 M. Dolg, H. Stoll, H. Preuss and R. M. Pitzer, *J. Phys. Chem.* 1993, **97**, 5852–5859.
- 56 S. Miertus, E. Scrocco and J. Tomasi, *Chem. Phys.* 1981, **55**, 117–129.
- 57 J. Tomasi, B. Mennucci and R. Cammi, *Chem. Rev.* 2005, **105**, 2999–3093.
- 58 P. E. Schwenn, P. L. Burn and B. J. Powell, *Org. Electron.* 2011, **12**, 394–403.
- 59 G. Audi and A. H. Wapstra, *Nucl. Phys. A* 1993, **565**, 1–65.
- 60 S. S. S. Raj, I. A. Razak, H-k. Fun, P-S. Zhao, F. Jiang, X. Yang, L. Lu and X. Wang, *Acta Cryst.* 2000, **C56**, e130–e131.
- 61 C. Engeker, H. E. Jackson, C. L. Knight and D. A. Thornton, *J. Mol. Struct.* 1989, **213**, 133–144.
- 62 D. A. Thornton, *Vibr. Spectroscopy* 1993, **4**, 309-319.
- 63 R. Marchon, L. Bokobza, G. Cote, *Spectrochim. Acta A* 1986, **42A**, 537–542.
- 64 A. D. Esposti, M. Brinkman and G. Ruani, *J. Chem. Phys.* 2002, **116**, 798–813.

- 65 C. C. Wagner, A. C. González-Baró and E. J. Baran, *Spectrochim. Acta Part A*, 2011, **78**, 1762–1765.
- 66 E. K. Plyler, *J. Res. Natl. Bureau Standards* 1952, **48**, 281–286.
- 67 J. Kidrič, D. Hadži, D. Krocjan and V. Rutar, *Org. Magn. Res.* 1981, **15**, 280–284.
- 68 D. R. Eaton, *J. Am. Chem. Soc.* 1965, **87**, 3097–3102.
- 69 B. Pritchard and J. Autschbach, *Inorg. Chem.* 2012, **51**, 8340–8351.
- 70 D-Xi Li, D.-J. Xu and Y-Zhi Xu, *Acta Cryst.* 2003, **E59**, m271-m272.
- 71 A. L. Spek, *J. Appl. Cryst.* 2003, **36**, 7–13.
- 72 F. Jensen, *Introduction to Computational Chemistry*, Wiley, England, 2nd edn., 2007, ch. 3, p. 93.
- 73 M. C. Stević, L. M. Ignjatović, G. Ćirić-Marjanović, S. M. Stanišić, D. M. Stanković and J. Zima, *Int. J. Electrochem. Sci.* 2011, **6**, 2509–2525.
- 74 F. Papadimitrakopoulos, X.-M. Zhang, D. L. Thompson and K. A. Higginson, *Chem. Mater.* 1996, **8**, 1363–1365.
- 75 P. I. Djurovich, E. I. Mayo, S. R. Forrest and M. E. Thompson, *Org. Electron.* 2009, **10**, 515–250.
- 76 V. V. N. Ravi Kishore, A. Aziz, K.L. Narasimhan, N. Periasamy, P.S. Meenakshi and S. Wategaonkar, *Synth. Met.* 2002, **126**, 199-205.
- 77 B. Bosnich, *J. Am. Chem. Soc.* 1968, **90**, 627–632.
- 78 F. E. Lytle, D. R. Storey and M. E. Juricich, *Spectrochim. Acta, Part A*, **1973**, **29**, 1357–1369.
- 79 C. H. Chen, J. Shi, *Coord. Chem, Rev.* 1998, **171**, 161–174.
- 80 M. L. Ramos, L. L. G. Justino, S. M. Fonseca and H. D. Burrows, *New J. Chem.* 2015, **39**, 1488-1497.

Table of Contents Entry

Synthesis, structure, spectral and electrochemical properties of chromium(III) *tris*-(8-hydroxyquinolate)

Ana R. Freitas, Mónica Silva, M. Luísa Ramos, Licínia L. G. Justino, Sofia M. Fonseca, Madalina M. Barsan, Christopher M. A. Brett, M. Ramos Silva, Hugh D. Burrows*



NMR spectra and DFT calculations show the chromium(III) *tris*-(8-hydroxyquinolate) HOMO predominantly involves metal 3d orbitals while the LUMO is mainly ligand based. This increases electrochemical stability of the metal quinolate.